P_{II}-like signaling protein SbtB links cAMP sensing with cyanobacterial inorganic carbon response

Khaled A. Selim[a,b,1], Florian Haase[c], Marcus D. Hartmann[b], Martin Hagemann[c], and Karl Forchhammer[a,1]

[a]Organismic Interactions Department, Interfaculty Institute for Microbiology and Infection Medicine, Tübingen University, 72076 Tübingen, Germany; [b]Department of Protein Evolution, Max Planck Institute for Developmental Biology, 72076 Tübingen, Germany; and [c]Plant Physiology Department, Institute of Biological Sciences, Rostock University, 18059 Rostock, Germany

Edited by Susan S. Golden, University of California, San Diego, La Jolla, CA, and approved April 9, 2018 (received for review March 7, 2018)

Cyanobacteria are phototrophic prokaryotes that evolved oxygenic photosynthesis ∼2.7 billion y ago and are presently responsible for ∼10% of total global photosynthetic production. To cope with the evolutionary pressure of dropping ambient CO_2 concentrations, they evolved a CO_2-concentrating mechanism (CCM) to augment intracellular inorganic carbon (C_i) levels for efficient CO_2 fixation. However, how cyanobacteria sense the fluctuation in C_i is poorly understood. Here we present biochemical, structural, and physiological insights into SbtB, a unique P_{II}-like signaling protein, which provides new insights into C_i sensing. SbtB is highly conserved in cyanobacteria and is coexpressed with CCM genes. The SbtB protein from the cyanobacterium *Synechocystis* sp. PCC 6803 bound a variety of adenosine nucleotides, including the second messenger cAMP. Cocrystal structures unraveled the individual binding modes of trimeric SbtB with AMP and cAMP. The nucleotide-binding pocket is located between the subunit clefts of SbtB, perfectly matching the structure of canonical P_{II} proteins. This clearly indicates that proteins of the P_{II} superfamily arose from a common ancestor, whose structurally conserved nucleotide-binding pocket has evolved to sense different adenyl nucleotides for various signaling functions. Moreover, we provide physiological and biochemical evidence for the involvement of SbtB in C_i acclimation. Collectively, our results suggest that SbtB acts as a C_i sensor protein via cAMP binding, highlighting an evolutionarily conserved role for cAMP in signaling the cellular carbon status.

P_{II}-like protein SbtB | signal transduction | inorganic carbon signaling | cAMP | cyanobacteria

Cyanobacteria evolved oxygenic photosynthesis about 2.7 billion y ago. This ability was later transmitted to eukaryotes via endosymbiosis, giving rise to plastids in algae and plants (1). The global proliferation of oxygenic photosynthetic conversion of C_i (CO_2 and HCO_3^-) into organic matter using light energy and electrons from water splitting led over time to a strong decline in available C_i on Earth. As a consequence, cyanobacteria evolved a CO_2-concentrating mechanism (CCM) that allows them to grow in the present-day atmosphere of the Earth, which contains only 0.04% CO_2 (2, 3).

The cyanobacterial CCM consists of several systems for C_i uptake as well as of the carboxysome, a proteinaceous bacterial cellular compartment in which the CO_2-fixing enzyme RubisCO and carbonic anhydrase (CA) are localized. The C_i-uptake systems concentrate massive amounts of bicarbonate inside the cyanobacterial cells, which then diffuses into the carboxysome, where CA converts it to CO_2. This strategy increases the CO_2 concentration in the vicinity of RubisCO, thereby saturating the carboxylation activity and minimizing the competing oxygenation reaction of this enzyme (2, 3). Therefore, the ability to respond to fluctuating C_i supply is of key importance, but the underlying mechanisms are still poorly understood.

The cyanobacterial bicarbonate transporter SbtA (4), as part of the CCM, is encoded in a bicistronic operon, together with the downstream gene *sbtB*; this operon is highly expressed with other CCM genes under C_i-limiting conditions (5, 6). In *Escherichia coli* cells expressing cyanobacterial *sbtA* and *sbtB*, SbtB inhibits SbtA-mediated HCO_3^- uptake (7). SbtB has been identified as a noncanonical member of the P_{II} signal transduction superfamily (8). P_{II} proteins are among the most widespread signaling proteins in nature. Canonical P_{II} proteins regulate nitrogen assimilation reactions by sensing the metabolic state of the cells through binding of small effector molecules [2-oxoglutarate (2-OG) and ATP/ADP]. This induces conformational changes in the large T loop that changes P_{II} interactions with target proteins, thereby modulating their activities. However, although members of the P_{II} superfamily are highly conserved in structure, they are very divergent in sequence, such that P_{II}-like proteins usually have low sequence identity and lack multiple consensus sequence motifs of canonical P_{II} proteins (8). The cognate effector molecules and biological functions of most P_{II}-like proteins, such as SbtB, are unknown. Here we analyzed the sensing properties and regulatory features of SbtB from *Synechocystis* sp. PCC 6803 (*Sc*SbtB).

Results

Biochemical Properties of *Sc*SbtB. Analysis of the *Sc*SbtB amino acid sequence (*SI Appendix*, *Bioinformatics Analysis* and Fig. S1 *A* and *B*) revealed the absence of virtually all residues known to

Significance

Life on Earth depends on photosynthetic CO_2 fixation to form organic carbon. This process evolved in cyanobacteria and was later conveyed to eukaryotes, giving rise to plastids in algae and plants. To cope with low atmospheric CO_2 concentrations that developed over the course of evolution, cyanobacteria evolved a CO_2-concentrating mechanism (CCM), which elevates CO_2 levels in the vicinity of RubisCO, the key enzyme of CO_2 fixation. Here we describe a conserved cyclic AMP receptor protein, SbtB, which participates in the sensing of fluctuating C_i levels to regulate the cyanobacterial CCM system. SbtB represents a new principle of C_i sensing, which is important for acclimation to varying C_i regimes in the ecological niches of cyanobacteria.

Author contributions: K.A.S., M.D.H., M.H., and K.F. designed research; K.A.S. performed biochemical, structural, and biophysical experiments; K.A.S. and F.H. performed physiological experiments; K.A.S., M.D.H., M.H., and K.F. analyzed data; and K.A.S., M.D.H., M.H., and K.F. wrote the manuscript.

The authors declare no conflict of interest.

This article is a PNAS Direct Submission.

Data deposition: Crystallography, atomic coordinates, and structure factors have been deposited in the Protein Data Bank, www.wwpdb.org (PDB ID codes 5O3P, 5O3Q, 5O3R, and 5O3S).

[1]To whom correspondence may be addressed. Email: khaled.selim@uni-tuebingen.de or karl.forchhammer@uni-tuebingen.de.

This article contains supporting information online at www.pnas.org/lookup/suppl/doi:10.1073/pnas.1803790115/-/DCSupplemental.

Published online May 7, 2018.

interact with 2-OG or the β- and γ-phosphates of the effector nucleotides (ATP/ADP) of canonical P_{II} proteins, which suggests that SbtB evolved sensory properties distinct from those of canonical P_{II} proteins. To identify potential sensing properties and regulatory features of SbtB, we prepared a recombinant *Sc*SbtB protein in its native trimeric state (*SI Appendix*, Fig. S1 *C–E*) and set out to address the question of potential metabolite binding using isothermal titration calorimetry (ITC) and microscale thermophoresis (MST).

We first tested the binding of the typical P_{II} effectors ATP, ADP, and 2-OG. While 2-OG binding was not detected (*SI Appendix*, Fig. S2), both ATP and ADP bound with comparably high affinities in the micromolar range (Table 1), even though SbtB lacks the canonical core residues for β- and γ-phosphate coordination. This led us to test for the binding of adenosine and AMP, which represent the core moiety for which large parts of the binding site appeared to be conserved. Binding of adenosine was weak (*SI Appendix*, Fig. S2), and AMP bound with an affinity only slightly lower than that of ATP and ADP, which suggested that AMP is the minimal binding moiety that is specifically recognized (*SI Appendix*, Fig. S2 *A–C*). We then checked for the binding of cAMP, which surprisingly bound with the highest affinity of all compounds tested (*SI Appendix*, Fig. S2*D*). Moreover, the binding enthalpy for cAMP was higher than that of the other nucleotides at the same concentration (compare *SI Appendix*, Fig. S2*E* with *SI Appendix*, Fig. S2 *A–C*), which indicated that binding cAMP is preferred over the other nucleotides. The guanosine nucleotides GTP and cGMP did not bind to *Sc*SbtB (*SI Appendix*, Fig. S2). For all nucleotides, a comparison of the calculated affinities using a model of three binding sites showed that the first two sites have similar affinities, whereas the third site is occupied with an approximately 10-fold lower affinity, which is indicative of anticooperativity (Table 1), like the canonical P_{II} protein (9, 10). The K_d values obtained by the MST measurements were in good qualitative agreement with the ITC data (Fig. 1*A* and Table 1).

The recent characterization of the P_{II}-like protein associated with carboxysomes from *Thiomonas intermedia* (*Ti*CP_{II}), whose gene is located near the *sbtAB* operon in many chemoautotrophic bacteria, provided clues that bicarbonate, AMP, and ADP are ligands (11). In addition, the binding of the adenosine nucleotides to *Ti*CP_{II} is stimulated 15-fold by 50 mM bicarbonate (11). Therefore, we also tested the effect of bicarbonate on *Sc*SbtB. Bicarbonate (50 mM) did not bind to *Sc*SbtB (*SI Appendix*, Fig. S2) or significantly influence the binding properties of the verified ligands (Table 1). To ensure that binding of cAMP is unique to *Sc*SbtB and not an overlooked property of canonical P_{II} proteins, we titrated cAMP and AMP against the *Synechococcus elongatus* P_{II} protein (*Se*P_{II}) without detecting any binding (*SI Appendix*, Fig. S2 *L* and *M*).

Structural Characterization of *Sc*SbtB. To determine the structural basis for ligand binding, *Sc*SbtB in apo form and in complex with AMP, ADP, or cAMP was crystallized, all rewarding well-diffracting crystals. The apo protein yielded a trigonal crystal form of space group $P3_2$. We solved its structure by molecular replacement using the *Anabaena variabilis SbtB* structure [*Av*SbtB; Protein Data Bank (PDB) ID code 3DFE] as a search model (*SI Appendix*, *Structural Characterization of* Sc*SbtB*). As expected, the refined apo-*Sc*Sbtb structure shows a canonical P_{II} ferredoxin-like fold (Fig. 1 *B* and *C*). All three subunits of the trimer are essentially in the same conformation, and the entire *Sc*SbtB trimer superimposes with Cα rmsd values of 0.53 Å on the *Av*SbtB trimer and 0.93 Å on the canonical *Se*P_{II} trimer (PDB ID code 2XUL) (*SI Appendix*, Figs. S3 and S4*A*). As in essentially all other crystal structures of isolated trimers of the P_{II} superfamily, the flexible T loop was mostly disordered (Fig. 1*C*).

Notable overall differences from the structures of canonical P_{II} proteins are found at the N and C termini. At the N terminus, the first β-strand runs antiparallel along the full length of the β4-strand to face the C terminus (Fig. 1*C*). The C terminus features a unique extension, which was unresolved in the *Av*SbtB structure but is fully ordered here. It forms a single α-helical turn flanking the canonical nucleotide-binding cleft, followed by a short hairpin loop formed by a CGPxGC motif, which is conserved in SbtB proteins (*SI Appendix*, Fig. S1 *A* and *B*), in which the two cysteines form a disulfide bridge (Fig. 1*C*). The carboxyl terminus of the last cysteine forms a hydrogen bond with the amino terminus. This mutually stabilizing interaction between the *Sc*SbtB N and C termini is shown in detail in Fig. 1*C*. The whole structural motif is invariant in all three chains of the trimer, which underpins its relevance.

Structural Characterization of Ligand Binding. Cocrystals of *Sc*SbtB with AMP, ADP, or cAMP yielded the same trigonal crystal form as for apo-*Sc*SbtB, and the same crystals were obtained in the presence and absence of bicarbonate. We solved the structures

Table 1. Dissociation constants calculated for binding of the adenyl nucleotides ATP, ADP, AMP, cAMP, and adenosine to the SbtB protein measured by ITC and MST

	ITC			MST
Titrant/Protein	K_{d1}, μM	K_{d2}, μM	K_{d3}, μM	K_d, μM
ATP				
SbtB	22.0 ± 1.0	6.9 ± 1.5	158.6 ± 23.8	46.0 ± 7.0
SbtB + 50 mM HCO_3^-	11.7 ± 0.2	5.6 ± 0.8	103.9 ± 1.9	NA
ADP				
SbtB	7.6 ± 1.0	9.3 ± 3.5	150.6 ± 18.8	18.9 ± 3.7
SbtB + 50 mM HCO_3^-	9.1 ± 2.3	7.2 ± 0.04	127.1 ± 13.4	NA
AMP				
SbtB	10.1 ± 1.1	7.4 ± 0.3	244.9 ± 9.8	70.4 ± 7.9
SbtB + 50 mM HCO_3^-	29.9 ± 33.8	16.1 ± 13.5	173.6 ± 20.3	NA
cAMP				
SbtB	2.1 ± 0.6	12.6 ± 2.5	76.2 ± 11.9	11.0 ± 1.9
SbtB + 50 mM HCO_3^-	3.9 ± 0.4	6.2 ± 1.2	86.8 ± 28.4	NA
Adenosine/SbtB		Weak binding		1,800.0 ± 1,530.0

The ITC K_d values were assayed in the presence or absence of 50 mM HCO_3^-. The raw ITC data were fitted to a model of three sequential binding sites for trimeric *Sc*SbtB. The K_d values correspond to the mean of the independent experiments ± SD. NA, not tested.

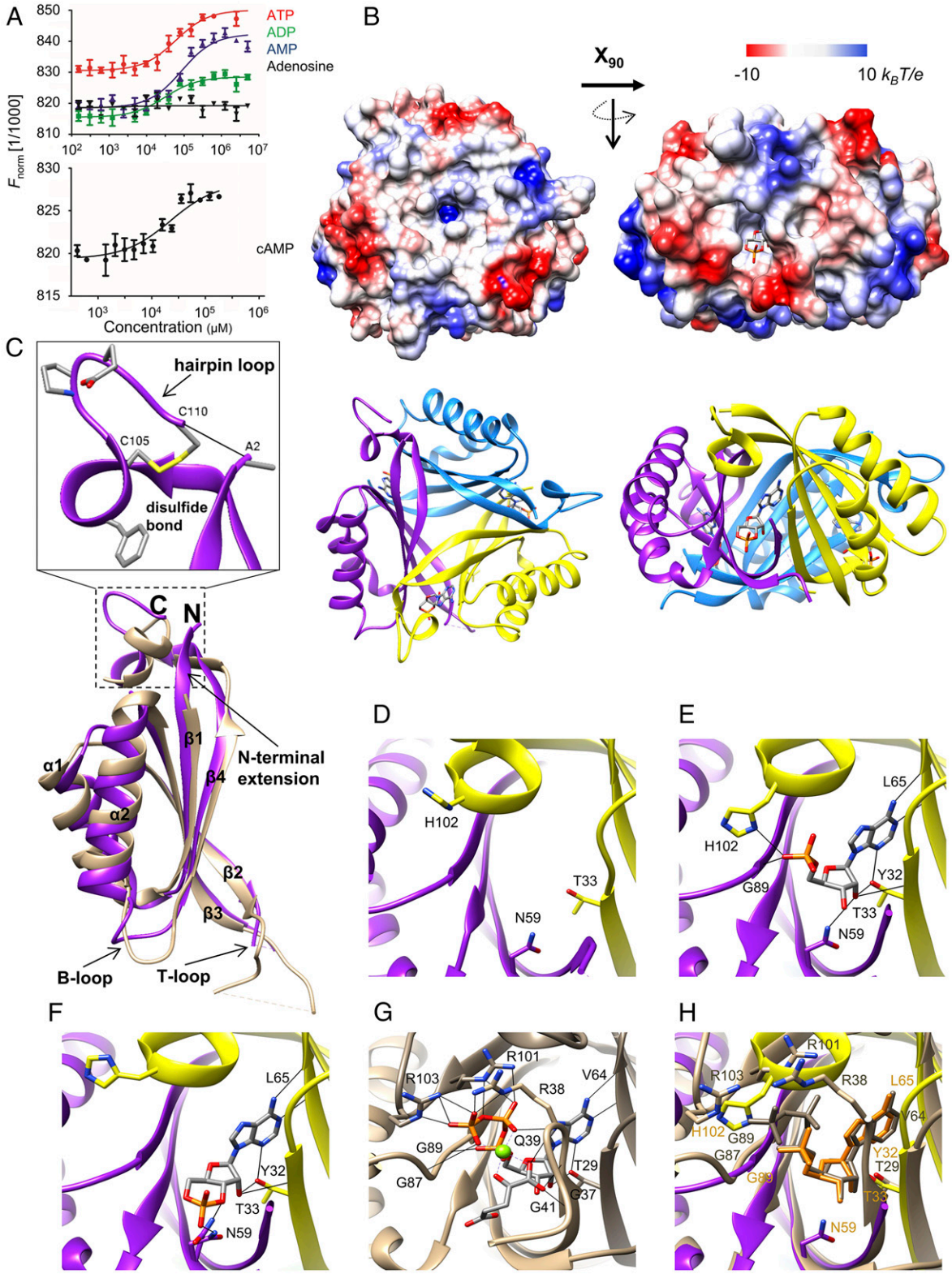

Fig. 1. Structural and binding properties of the *Sc*SbtB protein. (*A*) Binding of nucleotides monitored by MST ($n = 3$). (*A*, *Upper*) Titration series of ATP, ADP, AMP, and adenosine. (*A*, *Lower*) Titration series of cAMP. (*B*) Overall architecture of the SbtB protein. The structure of the trimeric SbtB–cAMP complex is shown as an electrostatic potential surface (*Upper*) and as a cartoon (*Lower*). The red–white–blue color gradient corresponds to surface potential values ranging from −10 to +10 k_BT/e. The structure of SbtB reveals the typical ferredoxin-like fold of the P_{II} superfamily, with nucleotide-binding pockets situated between the clefts of the subunits. (*C*) Superposition of monomeric subunits of SbtB (violet) with *Se*P_{II} (brown; PDB ID code 2XUL), yielding a 0.93-Å rmsd, with secondary structure elements and characteristic structural motifs indicated. (*C*, *Inset*) Highlighting of the hairpin-loop (CGPEGC) motif of SbtB with the disulfide bond between C105 and C110 and the hydrogen bond to the N terminus. (*D*–*G*) Close-up of the nucleotide binding site of the apo-SbtB, SbtB–AMP, SbtB–cAMP, and *Se*P_{II}–ATP structures, respectively. Relevant residues for nucleotide binding are shown as sticks, and H bonds are indicated by thin lines. (*H*) Superposition of the SbtB–AMP (yellow–violet) and *Se*P_{II}–ATP (brown) nucleotide binding sites, with relevant residues labeled in orange and dark brown, respectively.

on the basis of the apo-*Sc*SbtB coordinates; in all cocrystal structures, the electron density of the respective nucleotide was clear (*SI Appendix*, Fig. S4*B*). Structures of crystals grown in the presence or absence of bicarbonate did not differ, in agreement with the negligible influence of bicarbonate on the ITC measurements, which further confirms that the sensory properties of *Sc*SbtB differ from those of *Ti*CP$_{II}$ (11).

To our surprise, however, not only in the *Sc*SbtB–AMP structure but also in the putative *Sc*SbtB–ADP structure, only AMP was complexed, with clearly no electron density for a β-phosphate. Consequently, these two structures are virtually identical. The AMP moiety is bound as in most other known nucleotide-bound structures of the P$_{II}$ superfamily (Fig. 1 *D*–*H*). Specifically, the adenosine moiety forms hydrogen bonds to the backbone of L65 and the T33 side chain, and the phosphate forms a hydrogen bond to G89. Additional *Sc*SbtB-specific hydrogen bonds are formed between the ribose hydroxyl groups and the side chain of N59, which is only conserved in *Sc*SbtB, in the β-strand (β3) following the T loop. In two chains of the trimer, another bond is observed between the phosphate and a histidine (H102) in the C extension (Fig. 1*E*).

Due to the cyclic nature of cAMP, its phosphate binding mode differs from that of AMP. While the interactions of the adenine and ribose moieties of cAMP are the same as in the *Sc*SbtB–AMP structure, no bonds are formed between the phosphate and G89 or H102. Instead, at least in one binding site, the phosphate forms an additional hydrogen bond with N59 (Fig. 1*F*). All residues involved in nucleotide binding are shown in detail in *SI Appendix*, Fig. S4*B*.

ScSbtB Reversibly Associates with Membranes in an SbtA-Dependent Manner. *Sc*SbtB-specific antibodies (*SI Appendix*, Fig. S5*A*) were raised to reveal the subcellular localization and expression pattern of *Sc*SbtB in response to different treatments, showing that *Sc*SbtB accumulates in stationary-phase and carbon-limited conditions (*SI Appendix*, *Conditions Triggering SbtB Accumulation* and Fig. S5). It has been reported that when *sbtB* and *sbtA* are coexpressed in *E. coli*, SbtB tunes down SbtA-dependent HCO_3^- uptake (7). If the two proteins interact in wild-type *Synechocystis* sp. PCC 6803 cells (hereinafter WT), then SbtB should colocalize with the integral membrane protein SbtA. In WT cultures grown with low carbon (ambient air; hereinafter LC), SbtB was equally distributed between the membrane and soluble (cytosolic) fractions (Fig. 2*A*, *Left*). When cells were exposed to harsh C$_i$ starvation by omitting any gas exchange for 24 h (stationary culture flasks without aeration), SbtB was mainly in the membrane fraction (Fig. 2*A*, *Right*). By contrast, in an SbtA-deficient mutant, SbtB was exclusively soluble and never membrane-associated (Fig. 2*B*), which indicates that SbtA is required for SbtB membrane localization. To determine the dynamics of SbtB association/dissociation to/from the membrane, a WT culture grown with high carbon (5% CO_2; hereinafter HC) was shifted to LC conditions. At the start of the experiment (T_{zero}), SbtB was detected exclusively in the soluble fraction. One hour after the shift, the first traces of membrane-localized SbtB were observed, and the membrane-bound SbtB fraction gradually increased over 6 h (Fig. 2*C*).

To determine whether the ligands cAMP, AMP, and ADP affect the membrane localization of SbtB, each ligand (2 mM) was separately added to extracts of WT cells grown with LC and the extracts were then fractionated into soluble and membrane fractions. In WT extracts without added ligand, SbtB was partially localized in the membrane. Addition of ADP or AMP clearly and markedly triggered membrane localization of SbtB, whereas cAMP did not cause membrane localization of SbtB (Fig. 2*D*). Hence, binding of ADP or AMP, in contrast to binding of cAMP, would be advantageous for SbtA–SbtB complex formation in the membrane.

We then created a cAMP-free mutant by knocking out *slr1991* (designated *cya1*), which encodes the soluble adenylyl cyclase (12) (*SI Appendix*, Fig. S6 *A* and *B*), and tested the effect on SbtB localization upon shifting from LC to HC conditions. Under LC conditions, the amount of SbtB associated with the membrane was similar in the Δ*cya1* mutant and the WT. However, after shifting to HC conditions, SbtB dissociated from the membrane in the WT but not in the Δ*cya1* mutant (Fig. 2*E*). This result indicates that SbtB in the Δ*cya1* mutant does not sense the HC signal, which suggests that cAMP represents the HC signal that leads to membrane dissociation of SbtB.

ScSbtB Is Required for Efficient C$_i$ Acclimation. To characterize the role of SbtB in the CCM, we generated a completely segregated *sbtB* knockout mutant (Δ*sbtB*) (*SI Appendix*, Figs. S5*A* and S6 *A* and *C*). On solid BG$_{11}$ agar medium at pH 8 and 9, the Δ*sbtB* mutant grew almost like the WT under HC/LC conditions, but growth was negatively affected only at pH 7 under LC conditions, where more C$_i$ is present in the form of CO_2 (Fig. 3*A*, *Left*). Similarly, the Δ*sbtB* mutant grew significantly slower than the WT in liquid cultures at pH 8 under LC conditions, but such a

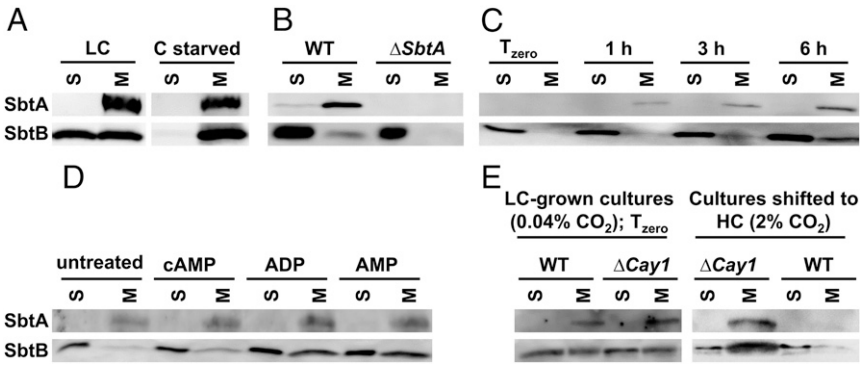

Fig. 2. Immunoblot analysis of SbtA-dependent *Sc*SbtB membrane localization. (*A*) Localization of SbtB in soluble (S) and membrane (M) fractions of cells grown with ambient air, that is, LC (0.04% CO_2; *Left*), or in carbon-starved cells (stationary culture flasks without aeration for 24 h; *Right*). (*B*) Distribution of SbtB between soluble and membrane fractions of WT and Δ*sbtA* mutant cells grown with LC (0.04% CO_2). SbtA antibodies were used to determine the quality of membrane isolation and the presence of SbtA. (*C*) Dynamics of SbtB membrane localization in WT cultures shifted from HC (5% CO_2) to LC (0.04% CO_2) for 1 to 6 h; T_{zero} represents HC conditions before the shift. (*D*) Influence of added nucleotides on SbtB localization. Crude cell extracts of cells grown under LC were prepared, the indicated nucleotide (2 mM) was then added separately to the extracts, and membrane and soluble fractions were separated. (*E*) SbtB localization in WT and Δ*cya1* mutant cells grown under LC (air-grown) and HC (2% CO_2) conditions as indicated. See *SI Appendix*, *Materials and Methods* for a detailed description of membrane fractionation.

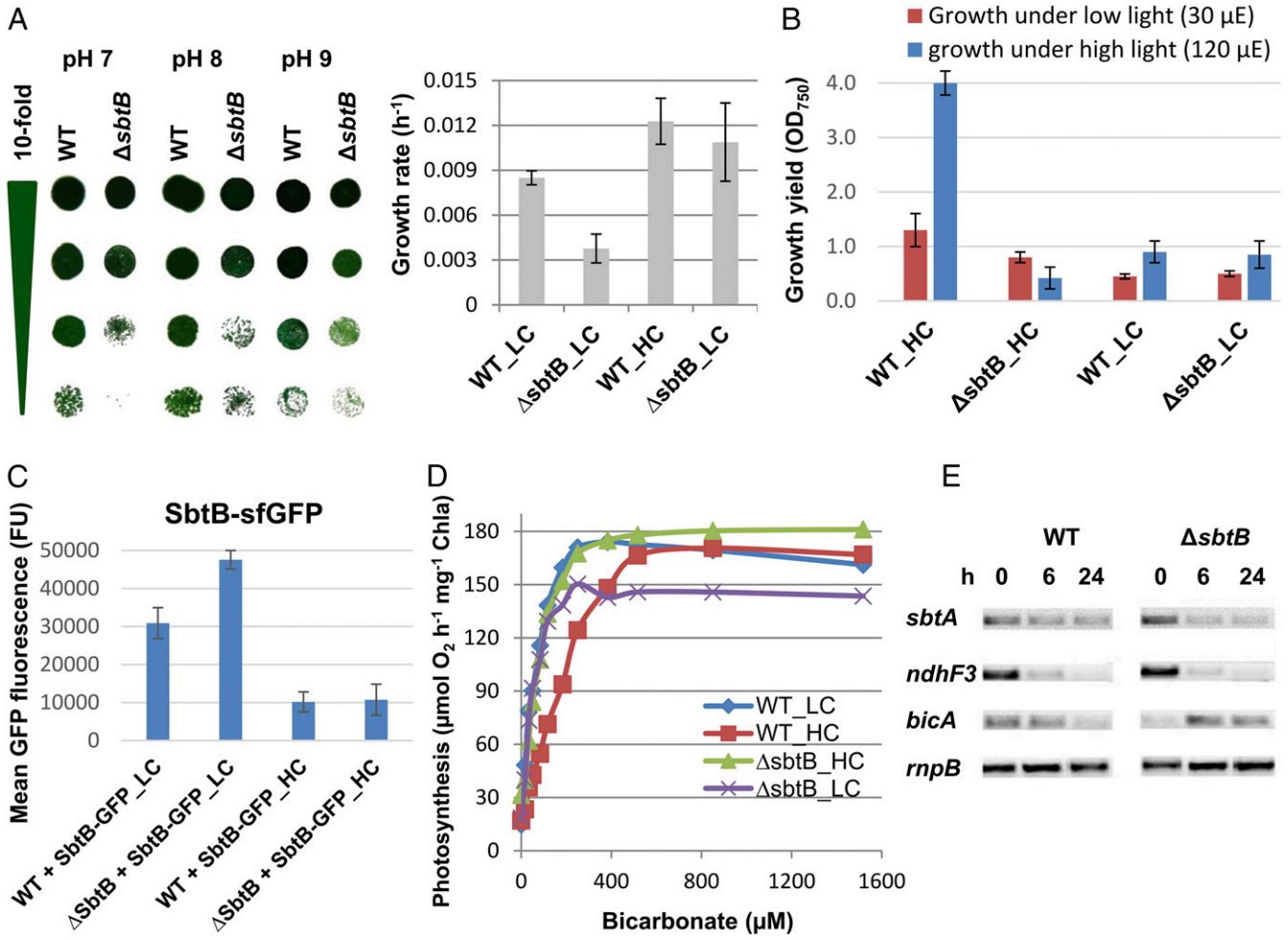

Fig. 3. Phenotypic characterization of the Δ*sbtB* knockout mutant. (*A*) Growth of WT or Δ*sbtB* mutant cells on solid BG_{11} medium at different pH values under LC conditions (*Left*) or in liquid BG_{11} medium at pH 8.0 under LC or HC conditions (*Right*, error bars represent standard deviations from three independent cultivation experiments). (*B*) Effect of sudden change in carbon supply in the form of growth yield. WT and the Δ*sbtB* mutant were shifted from slow-growing cultures (LC/low light, 30 µE) either to HC (2% CO_2) or LC (air) under the initial light intensity (30 µE), or to HC (5% CO_2) and LC (air) with increased light intensity (120 µE). (*C*) Levels of fluorescent SbtB-sfGFP protein in WT and the Δ*sbtB* complemented mutant in response to HC and LC growth (standard deviation; $n = 3$). (*D*) Bicarbonate-dependent photosynthetic rates per chlorophyll a (Chla) of WT and the Δ*sbtB* mutant as a function of increasing HCO_3^- concentrations. Cells were acclimated to either HC or LC conditions ($n = 3$). (*E*) Gene expression of selected CCM genes in WT and the Δ*sbtB* mutant analyzed using semiquantitative RT-PCR. Cells were cultivated under LC conditions (0 h) and then shifted to HC conditions (5% CO_2) for 24 h; the constitutively expressed *rnpB* gene served as loading control.

difference was not observed under HC conditions (Fig. 3*A*, *Right*). Importantly, Δ*sbtB* cells were highly sensitive to sudden changes in carbon supply; when slowly growing Δ*sbtB* mutant cells (LC and low light of 30 µE) were suddenly exposed to 2% CO_2 at the same light intensity, the culture temporarily ceased growth and only slowly recovered. This effect became even more pronounced at higher light intensity and with further CO_2 supplementation (5% CO_2, 120 µE). By contrast, WT cultures immediately increased growth at HC levels under low and high light intensity (Fig. 3*B* and *SI Appendix*, *Physiological Function of* Sc*SbtB* and Fig. S7*A*).

To complement the growth defect of Δ*sbtB*, a plasmid expressing the gene encoding an *Sc*SbtB-sfGFP (superfolded GFP) fusion protein under the control of the native promoter of the *sbt* operon was transformed into WT and Δ*sbtB* cells to generate the strains WT+SbtB-sfGFP and Δ*sbtB*+SbtB-sfGFP (*SI Appendix*, Fig. S6 *A* and *D*). To check the expression of the SbtB-sfGFP construct, we quantified SbtB-sfGFP fluorescence under HC and LC conditions (Fig. 3*C*). The GFP signal was much lower under HC conditions than under LC conditions, in agreement with the expression pattern of native SbtB in response to C_i (5, 6). Under LC, the SbtB-sfGFP signal was lower in the WT+SbtB-sfGFP strain than in the Δ*sbtB*+SbtB-sfGFP strain, which indicated that the genomic copies of *sbtB* (*slr1513*) in WT cells quench the expression of SbtB-sfGFP. Next, we tested whether the *Sc*SbtB-sfGFP construct complements the phenotype of the Δ*sbtB* mutant by analyzing acclimation to a shift in CO_2 levels as described above. Indeed, the SbtB-sfGFP construct complemented the growth defect of the Δ*sbtB* mutant (*SI Appendix*, Fig. S7 *A–D*), which demonstrated that SbtB-sfGFP was functionally active and that the growth defect of Δ*sbtB* was not caused by polar effects. Last, we determined the cellular localization of SbtB under HC and LC conditions by monitoring the sfGFP signals by fluorescence microscopy. Under HC conditions, the SbtB-sfGFP signal was mainly cytoplasmic. However, 1 h after the shift to LC conditions, SbtB-sfGFP partially relocalized to the cytoplasmic membrane (*SI Appendix*, Fig. S8). Together, these data suggest that SbtB is required to acclimate to sudden changes in CO_2 levels, which highlights its sensory/regulatory role in C_i acclimation.

To obtain further evidence for the proposed functional link between SbtB and control of C_i metabolism, we determined C_i-uptake

affinity from HC- and LC-acclimated cells by measuring the amount of oxygen evolved from HCO_3^--dependent photosynthesis. Intriguingly, the maximal photosynthetic rates of LC-acclimated Δ*sbtB* mutant cells were lower than those of the WT (Fig. 3*D*). The lower V_{max} indicates an impaired function of CO_2-fixing Calvin–Benson cycle activity, which limits the photosynthetic activity at saturating C_i amounts; this result is consistent with the slower growth of Δ*sbtB* under LC conditions. In contrast, the affinity toward bicarbonate was almost similar in WT and mutant Δ*sbtB* cells under LC conditions, since the initial rise in the photosynthetic activity was indistinguishable between these two strains. Strikingly, only WT cells showed the expected acclimation to HC conditions by lowering bicarbonate affinity (HCO_3^- K_m: LC, 48 μM; HC, 95 μM), whereas Δ*sbtB* cells retained the high C_i affinity under HC conditions (HCO_3^- K_m: LC, 52 μM; HC, 68 μM) (Fig. 3*D*). This behavior implies that Δ*sbtB* resides in the LC-adapted state even under HC conditions, and provides a rationale for the inability of the Δ*sbtB* mutant to rapidly acclimate to a CO_2 upshift (see above).

The inability of the Δ*sbtB* mutant to adjust the C_i affinity in response to the ambient CO_2 supply suggests that the SbtB protein plays a role in the regulation of the entire CCM, similar to the role of the canonical P_{II} protein in N assimilation (8, 13). To test whether the Δ*sbtB* mutation affects the expression of other C_i-controlled genes, we analyzed the transcript levels of CCM-related genes upon shifting cells from LC to HC. The genes coding for various C_i-uptake systems were highly expressed in WT and Δ*sbtB* mutant cells grown under LC conditions (Fig. 3*E*, time 0), and expression of *sbtA* and *ndhF3* markedly decreased upon shifting to HC conditions; *ndhF3* encodes a subunit of the inducible CO_2-uptake system NDH-I_3 (3, 14) (Fig. 3*E*, time points 6 and 24 h after shift). Since the abundance of *sbtA* mRNA was similar in the WT and Δ*sbtB* mutant, we can safely assume that the downstream *sbtB* gene mutation does not affect the expression of the upstream *sbtA* gene; this result agrees with a previous report that the inactivation of *sbtB* in *Synechococcus* sp. PCC 7942 does not affect the bicarbonate-uptake activity of SbtA (15). Surprisingly, the expression of another HCO_3^- transporter, *bicA* (16), was deregulated completely in Δ*sbtB*, whereas in the WT the expression was like that of *sbtA* (Fig. 3*E*), which indicates that the *sbtB* mutation might have a broader impact on C_i regulation than only the direct regulation of SbtA. The expression of the LC-inducible gene *bicA* under HC conditions agrees with the preacclimatization of the Δ*sbtB* mutant to LC conditions, and might be the cause of the inability of the Δ*sbtB* mutant to adapt C_i affinity to HC conditions.

cAMP/AMP as a C_i Signal Compete for *Sc*SbtB. To address whether the stably bound *Sc*SbtB effector molecules cAMP and AMP are related to fluctuations in C_i supply, we measured the cellular levels of cAMP and AMP in WT cells as a function of C_i. An HC-adapted culture was harvested, resuspended in fresh medium, and divided into two subcultures. One subculture was reincubated again under HC conditions, and the other subculture was incubated under LC conditions. After 30 min and 4 h, samples were taken, and the levels of cAMP and AMP were quantified. The AMP levels were 18- to 20-fold higher under LC conditions than under HC conditions. By contrast, cAMP showed the opposite trend, namely cAMP levels were 3- to 4-fold higher under HC conditions than under LC conditions (Fig. 4*A*).

To reveal whether these physiological changes in cAMP relative to AMP are functionally relevant for *Sc*SbtB signaling, we determined the competitive binding of cAMP and AMP to *Sc*SbtB using ITC. Under saturating concentrations of cAMP (300 μM), binding of AMP (2 mM) to *Sc*SbtB was completely inhibited (Fig. 4*B*). In the presence of 100 μM cAMP, AMP was able to bind only to the available unoccupied sites of *Sc*SbtB with low affinity (*SI Appendix*, Fig. S2*N*). The determined K_d value of 240.9 μM is similar to the third (low-affinity) binding site of AMP in trimeric *Sc*SbtB (compare with Table 1). However, when *Sc*SbtB was

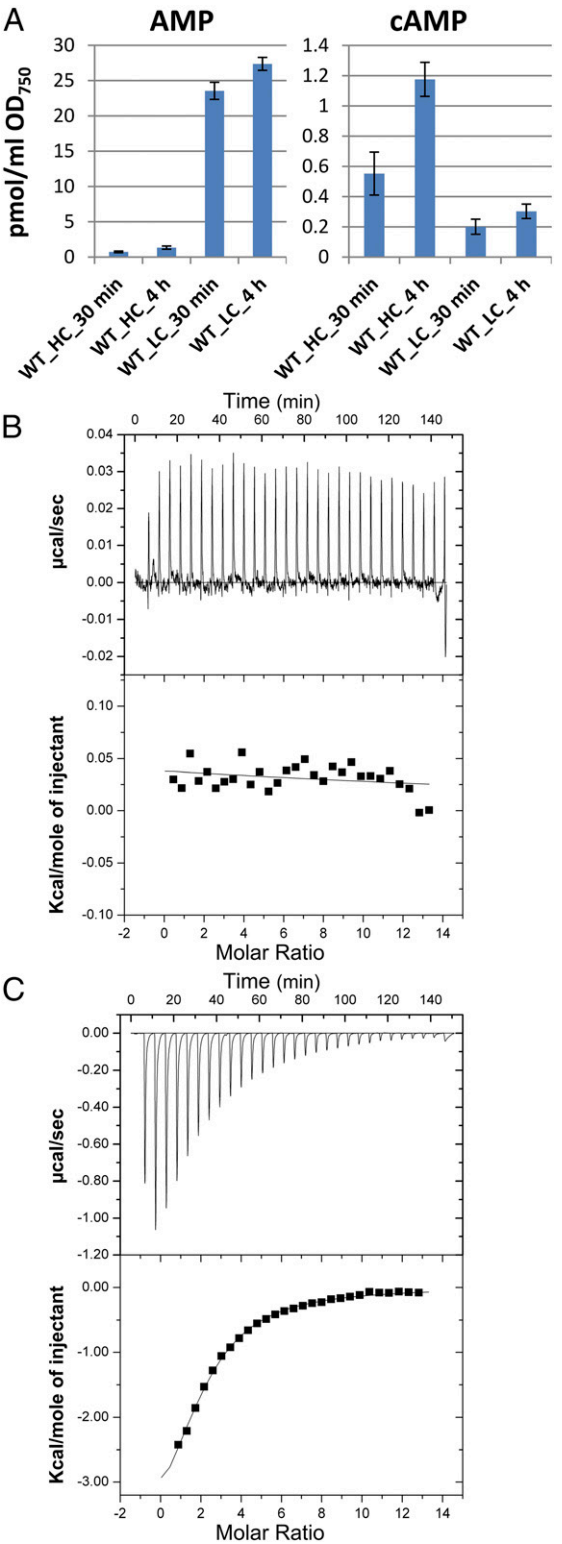

Fig. 4. Response of cAMP and AMP to cellular C_i levels, and competitive binding assay of cAMP and AMP to *Sc*SbtB. (*A*) Mean cellular levels and standard deviations ($n = 3$) of cAMP and AMP were determined under LC or HC conditions after 30 min and 4 h. (*B* and *C*) ITC titration of 33.3 μM SbtB (trimeric concentration) in the presence of (*B*) 300 μM cAMP against 2 mM AMP and (*C*) 300 μM AMP against 2 mM cAMP. (*B* and *C*, *Upper*) Raw ITC data in the form of the heat produced during the titration. (*B* and *C*, *Lower*) Binding isotherms and the best-fit curves according to the one–binding-site model for trimeric SbtB.

preincubated with 300 μM AMP, cAMP was still able to bind to *Sc*SbtB, with each injection (corresponding to ∼14 μM cAMP) producing a strong exothermic signal. The resulting isotherm could be fitted to an apparent K_d of 42.2 μM (Fig. 4*C*). Therefore, under HC conditions, with elevated levels of cAMP and highly diminished levels of AMP, we expect that *Sc*SbtB will accommodate cAMP. By contrast, under LC conditions, the increasing levels of AMP and concomitantly decreasing levels of cAMP will give rise to the AMP-bound state of *Sc*SbtB.

Discussion

Common properties of canonical P_{II} proteins are the competitive binding of the adenyl nucleotides ATP or ADP to sense the energy status of cells (8, 17) and the ATP-dependent binding of 2-OG as a status indicator of the cellular carbon–nitrogen balance. By contrast, the larger family of P_{II}-like proteins has different adenyl-nucleotide binding modes and does not generally bind 2-OG (8, 18). SbtB extends the range of sensing in the P_{II} superfamily. *Sc*SbtB is a unique member of the P_{II} superfamily for which specific binding of ATP, ADP, AMP, and cAMP has been described. In contrast to canonical PII proteins, the β- and γ-phosphates of the adenyl nucleotides seem of minor importance for SbtB binding and, accordingly, the interacting residues, such as the RxR motif in the C loop, are not conserved (*SI Appendix*, Fig. S1). However, the location of the nucleotide-binding pocket in the intersubunit clefts and the recognition mode of the nucleoside moiety are perfectly conserved with other members of the P_{II} superfamily (8) (Fig. 1*H*). This agrees with the assumption that proteins of the P_{II} superfamily arose from a common nucleotide-binding ancestor, whose binding pocket has been structurally conserved but whose binding mode has evolved to sense different adenyl nucleotides to fulfill various signaling functions (8).

Interestingly, when we solved the structure of the putative *Sc*SbtB–ADP complex, AMP was bound and there was clearly no electron density for a β-phosphate. A similar phenomenon has been reported for other members of the P_{II} superfamily (11, 19), but whether ADP is enzymatically hydrolyzed by *Sc*SbtB to AMP remains unclear.

An intriguing property of *Sc*SbtB is the presence of a conserved CGPxGC motif at the C terminus. This extension forms a small helix–hairpin loop structure, which forms a disulfide bond between cysteines C105 and C110. An identical C-terminal segment, CGPxGC, is also present in a subgroup of thiol disulfide oxidoreductases (DsbA). The members of this subgroup form dimers in which the CGPxGC terminus of one monomer is in close proximity to the catalytic CPxC motif. The structure of such a C terminus of a DsbA family protein (PDB ID code 3GL5) is almost identical to the hairpin-loop extension of *Sc*SbtB. Furthermore, many of the plant Calvin–Benson–cycle enzymes have evolved similar redox-regulated C-terminal extensions, C(V/I)VxVC, to modulate their activity through oxidation/reduction of intramolecular disulfide bridges under the different light conditions of day/night cycles (20, 21). Therefore, the hairpin-loop extension of SbtB might be involved in a redox-sensory function.

One of the most striking features of *Sc*SbtB is the binding of cAMP. Increasing evidence suggests that cAMP signaling plays an important role in C_i perception. The increased levels of cAMP under HC conditions agree with the finding that cyanobacterial soluble adenylyl cyclase activity is stimulated by elevated levels of C_i, which causes increased cAMP production (22–25). In diatoms, which possess CCMs, increasing CO_2 concentrations cause elevated cAMP levels, which induce down-regulation of the CCMs (26). Therefore, cAMP can be considered an evolutionarily conserved second messenger molecule that responds to C_i, thereby regulating CCMs in deeply branched phyla of cyanobacteria and algae. Another well-known regulatory nucleotide, the stringent control nucleotide ppGpp, was recently identified in cyanobacteria to control global gene expression during day/night switches (27, 28), emphasizing a fundamental role of secondary messenger nucleotides in the cyanobacteria lifestyle.

Although it has been recognized that cAMP is involved in carbon sensing, our results imply that the level of AMP might also play a role in C_i sensing. The levels of cAMP and AMP were similar in cells grown under HC conditions, whereas the cAMP-to-AMP ratio decreased ∼60- to 80-fold when cultures were shifted to LC conditions (Fig. 4). From this, we expect that under HC conditions, SbtB will preferentially bind cAMP over AMP, whereas under LC conditions, AMP will outcompete cAMP. In vitro, AMP favored the membrane-associated state of SbtB, whereas cAMP favored the soluble state. This perfectly agrees with the prevalence of cytoplasmic SbtB under HC conditions (high cAMP-to-AMP ratio) as opposed to membrane-associated SbtB in the LC state (low cAMP-to-AMP ratio). Structurally, there is no considerable difference between the AMP- and cAMP-bound SbtB conformations. However, it is conceivable that the bound nucleotides directly contribute to the interface between SbtA and SbtB, such that the open phosphate group of AMP stabilizes the complex, while cAMP disrupts the interface with its differently oriented phosphate.

*Sc*SbtB and the recently described *Ti*CP_{II} protein (PDB ID code 5DS7) both sense ADP and AMP (11), and superimpose closely with an rmsd of 0.9 Å (*SI Appendix*, Figs. S3*C* and S4*A*). However, *Ti*CP_{II} directly responds to HCO_3^- and thereby increases the affinity to the adenyl nucleotides (11), whereas *Sc*SbtB does not respond to HCO_3^-, its affinity to adenyl nucleotides is not influenced by high amounts of external bicarbonate levels (Table 1), and it senses cAMP as a second messenger of the cellular carbon supply. Since both P_{II}-like proteins respond to ADP/AMP, it appears that a central, yet not understood, task of these proteins is to link C_i assimilation to the energy and carbon states of the cells. However, the sensing of the C_i status occurs via distinct mechanisms. In the case of *Ti*CP_{II}, HCO_3^- is directly bound in the effector molecule binding site, thereby increasing the affinity by two orders of magnitude. By contrast, *Sc*SbtB perceives the carbon status indirectly, via the binding of the second messenger cAMP.

The phenotypic changes of the SbtB-deficient mutant suggest that SbtB is involved in the regulation of the cyanobacterial CCM, similar to the role of the canonical P_{II} protein in N assimilation (8, 13). Cells of the SbtB-deficient mutant seem to be locked in the LC-acclimated state even under HC conditions. Gene expression analysis revealed that the *sbtB* deletion had no impact on HC-induced repression of the upstream *sbtA* gene, whereas expression of the *bicA* gene encoding another bicarbonate transporter differed in WT and mutant cells. Currently, we have no mechanistic explanation for this finding, but it indicates that different factors are involved in the regulation of *bicA* and the *sbt* operon, with *bicA* expression being dependent on SbtB. Therefore, in addition to a direct regulation of SbtA transport activity (7), SbtB might be involved in a more general regulation of the CCM, in analogy to the multiple functions of canonical cyanobacterial P_{II} proteins in metabolic regulation (29).

Under conditions of C_i starvation, SbtA and SbtB were produced at the highest levels, and SbtB was bound to the membrane via SbtA. Under these conditions, maximal activity of SbtA is required to keep the intracellular bicarbonate level high. Consequently, this SbtA–SbtB complex must be active in bicarbonate transport and, therefore, binding of SbtB does not necessarily inhibit SbtA activity. This clearly distinguishes SbtB from the P_{II} protein GlnK, which associates with the ammonium channel protein Amt to close the pores and shut down the uptake of ammonia (30, 31). It is, however, possible that SbtB switches off SbtA activity during the night, possibly involving the C terminus of *Sc*SbtB, which is likely redox-regulated. Another purpose of SbtB binding to SbtA could be to stabilize SbtA or to sequester SbtB to the membrane and thereby exert a regulatory function, similar to that shown for the regulation of nitrogenase-associated DraG/DraT by

P_{II} proteins in *Azospirillum brasilense* (32). If soluble SbtB interacts with a regulator that mediates acclimation to high CO_2 levels, then deletion of SbtB could lock the cells in the LC-adapted state.

Collectively, our findings extend the knowledge on cAMP sensing. While the sensing of organic carbon (glucose) by cAMP is well-understood, a mechanistic link for the thus far unclear relationship between cAMP and C_i sensing has been enigmatic. The P_{II}-like signaling protein SbtB represents a novel type of cAMP receptor protein and perceives C_i status via binding of the second messenger cAMP. In eukaryotes, cAMP transmits signals that originate at G protein-coupled receptors and modulate cellular activities mainly through cAMP-dependent protein kinases (33), thereby affecting gene expression or central metabolism, in particular glycogen, sugar, and lipid metabolism. In bacteria, cAMP mediates manifold cellular responses, mainly via cAMP-responsive transcription factors, such as CRP (34, 35), but also via cAMP-controlled protein modification enzymes, such as protein kinases and GNAT-related protein lysine acetylases (36). With SbtB, a novel mechanism of cAMP-mediated signaling in cyanobacterial carbon regulation has been unraveled, and a functional link between CO_2 acquisition and cAMP sensing has been revealed. However, further studies are required to mechanistically understand the interaction with the target SbtA as well as the interplay between the various adenyl-nucleotide effector molecules for energy and carbon sensing.

Materials and Methods

Full protocols are available in *SI Appendix, Materials and Methods*.

Purification of Recombinant Proteins. Recombinant C-terminal StrepII-tagged proteins (*Sc*SbtB and canonical *Se*P_{II}) were purified as previously described (9, 10).

Determination of *Sc*SbtB Binding Constants. *Sc*SbtB binding constants were determined using ITC (VP-ITC microcalorimeter; MicroCal) and MST (Monolith NT.LabelFree; NanoTemper Technologies). The ITC binding isotherms were calculated from the recorded data and fitted to one-site and three-site binding models using MicroCal Origin software (10). MST single-site fitting was done using NanoTemper data analysis software.

Crystallization, Data Collection, and Structure Elucidation. Proteins were crystallized via vapor diffusion at 20 °C in 96-well sitting-drop plates. The structure of apo-*Sc*SbtB was solved by molecular replacement using MOLREP (37) and the *Av*SbtB structure (PDB ID code 3DFE) as a search model. Other structures were solved subsequently on the basis of the apo-*Sc*SbtB coordinates (PDB ID code 5O3P). Structural representations were prepared using UCSF Chimera (https://www.cgl.ucsf.edu/chimera/).

Generation of Mutants. Knockout deletion mutants were constructed by cloning the upstream and downstream regions of the ORF *slr1513* (designated *sbtB*) (4, 5) and the ORF *slr1991* (designated *cya1*) (12) with the erythromycin resistance cassette (primers are listed in *SI Appendix*, Table S1). For complementation, SbtB-sfGFP strains were generated by introducing the *sbtB* gene (*slr1513*) fused to the gene encoding sfGFP into Δ*sbtB* and WT backgrounds using the self-replicating plasmid pVZ322.

CO_2-Shift Experiments. CO_2-shift experiments were performed according to ref. 38. Briefly, cells were precultured in standard BG_{11} medium (pH 8) with bubbling of air-enriched CO_2 [2 to 5% (vol/vol); defined as high-carbon conditions] at a light intensity of about 100 μE. Cells were shifted to low CO_2 by bubbling with ambient air [0.04% (vol/vol) CO_2; defined as low-carbon conditions]. For a harsh carbon shift, cells were transferred to BG_{11} medium free of HCO_3^- and CO_3^{-2} and kept stationary. For a shift to HC conditions, the gas stream of LC-grown cells was switched from ambient air to CO_2-supplemented air.

Phenotypic Characterization of the Δ*sbtB* Mutant. Wild-type *Synechocystis* sp. PCC 6803 and Δ*sbtB* cells were grown under various CO_2 conditions as mentioned above. The survival of cells was checked in standard BG_{11} medium in a drop-dilution assay on agar plates of various pH and by measuring growth rates in liquid medium. The rate of C_i-dependent oxygen evolution as a function of increasing HCO_3^- supply was determined using a Clark-type oxygen electrode (Hansatech).

Transcriptional Analysis. Total RNA was isolated using the PGTX method (39). Reverse transcription was done using the RevertAid RT Kit (Thermo Fisher). Aliquots of the generated cDNA were used for the RT-PCR assays of selected C_i-regulated genes using gene-specific primers (*SI Appendix*, Table S1).

Quantification of cAMP and AMP. cAMP and AMP were extracted according to ref. 40. The intracellular levels of cAMP and AMP were analyzed and determined using the LCMS-8050 System and LC/MS/MS Method Package for Primary Metabolites version 2 (Shimadzu). For quantification of cAMP and AMP, authentic substances in appropriate concentrations were used for calibration.

Immunoblot Analysis of the Cellular Localization of *Sc*SbtB. For immunoblot analysis, the crude cell extract from WT cells grown in or shifted to different CO_2 conditions as indicated was prepared using a ribolyser for four cycles at 4 °C. For localization experiments, total cell extracts were fractionated into membranes and soluble fractions according to ref. 30.

ACKNOWLEDGMENTS. The authors are grateful to Reinhard Albrecht for crystallographic sample preparation and assistance with diffraction data collection, the staff of beamline X10SA/SLS, and Karen Brune for critical linguistic editing of the manuscript. M.D.H. gratefully acknowledges Andrei Lupas for continued support. K.A.S. and K.F. thank all members of the Organismic Interactions Department, especially Jan Lüddecke and Carolina Nishi, for technical assistance. This work was supported by Deutsche Forschungsgemeinschaft Grant Fo195/9-2, Graduiertenkolleg Grant 1708-2, and Deutsch Akademischer Austauschdienst (DAAD); the Hochschulbauförderungsgesetz (HBFG) program financed the LC/MS equipment (GZ: INST 264/125-1 FUGG).

1. Hohmann-Marriott MF, Blankenship RE (2011) Evolution of photosynthesis. *Annu Rev Plant Biol* 62:515–548.
2. Rae BD, Long BM, Badger MR, Price GD (2013) Functions, compositions, and evolution of the two types of carboxysomes: Polyhedral microcompartments that facilitate CO_2 fixation in cyanobacteria and some proteobacteria. *Microbiol Mol Biol Rev* 77: 357–379.
3. Burnap RL, Hagemann M, Kaplan A (2015) Regulation of CO_2 concentrating mechanism in cyanobacteria. *Life (Basel)* 5:348–371.
4. Shibata M, et al. (2002) Genes essential to sodium-dependent bicarbonate transport in cyanobacteria: Function and phylogenetic analysis. *J Biol Chem* 277:18658–18664.
5. Wang HL, Postier BL, Burnap RL (2004) Alterations in global patterns of gene expression in *Synechocystis* sp. PCC 6803 in response to inorganic carbon limitation and the inactivation of ndhR, a LysR family regulator. *J Biol Chem* 279:5739–5751.
6. Schwarz D, Schubert H, Georg J, Hess WR, Hagemann M (2013) The gene sml0013 of *Synechocystis* species strain PCC 6803 encodes for a novel subunit of the NAD(P)H oxidoreductase or complex I that is ubiquitously distributed among cyanobacteria. *Plant Physiol* 163:1191–1202.
7. Du J, Förster B, Rourke L, Howitt SM, Price GD (2014) Characterisation of cyanobacterial bicarbonate transporters in *E. coli* shows that SbtA homologs are functional in this heterologous expression system. *PLoS One* 9:e115905.
8. Forchhammer K, Lüddecke J (2016) Sensory properties of the P_{II} signalling protein family. *FEBS J* 283:425–437.
9. Fokina O, Chellamuthu VR, Zeth K, Forchhammer K (2010) A novel signal transduction protein P(II) variant from *Synechococcus elongatus* PCC 7942 indicates a two-step process for NAGK-P(II) complex formation. *J Mol Biol* 399:410–421.
10. Lapina T, Selim KA, Forchhammer K, Ermilova E (2018) The P_{II} signaling protein from red algae represents an evolutionary link between cyanobacterial and Chloroplastida P_{II} proteins. *Sci Rep* 8:790.
11. Wheatley NM, et al. (2016) A PII-like protein regulated by bicarbonate: Structural and biochemical studies of the carboxysome-associated CP_{II} protein. *J Mol Biol* 428:4013–4030.
12. Terauchi K, Ohmori M (1999) An adenylate cyclase, Cya1, regulates cell motility in the cyanobacterium *Synechocystis* sp. PCC 6803. *Plant Cell Physiol* 40:248–251.
13. Huergo LF, Chandra G, Merrick M (2013) P(II) signal transduction proteins: Nitrogen regulation and beyond. *FEMS Microbiol Rev* 37:251–283.
14. Shibata M, et al. (2001) Distinct constitutive and low-CO_2-induced CO_2 uptake systems in cyanobacteria: Genes involved and their phylogenetic relationship with homologous genes in other organisms. *Proc Natl Acad Sci USA* 98:11789–11794.
15. Price GD (2011) Inorganic carbon transporters of the cyanobacterial CO_2 concentrating mechanism. *Photosynth Res* 109:47–57.
16. Price GD, Woodger FJ, Badger MR, Howitt SM, Tucker L (2004) Identification of a SulP-type bicarbonate transporter in marine cyanobacteria. *Proc Natl Acad Sci USA* 101:18228–18233.
17. Lüddecke J, Forchhammer K (2015) Energy sensing versus 2-oxoglutarate dependent ATPase switch in the control of *Synechococcus* P_{II} interaction with its targets NAGK and PipX. *PLoS One* 10:e0137114.

18. Fokina O, Chellamuthu VR, Forchhammer K, Zeth K (2010) Mechanism of 2-oxoglutarate signaling by the *Synechococcus elongatus* P_{II} signal transduction protein. *Proc Natl Acad Sci USA* 107:19760–19765.
19. Radchenko MV, Thornton J, Merrick M (2013) P(II) signal transduction proteins are ATPases whose activity is regulated by 2-oxoglutarate. *Proc Natl Acad Sci USA* 110: 12948–12953.
20. Michelet L, et al. (2013) Redox regulation of the Calvin-Benson cycle: Something old, something new. *Front Plant Sci* 4:470.
21. Tamoi M, Shigeoka S (2015) Diversity of regulatory mechanisms of photosynthetic carbon metabolism in plants and algae. *Biosci Biotechnol Biochem* 79:870–876.
22. Chen Y, et al. (2000) Soluble adenylyl cyclase as an evolutionarily conserved bicarbonate sensor. *Science* 289:625–628.
23. Cann MJ, Hammer A, Zhou J, Kanacher T (2003) A defined subset of adenylyl cyclases is regulated by bicarbonate ion. *J Biol Chem* 278:35033–35038.
24. Steegborn C, Litvin TN, Levin LR, Buck J, Wu H (2005) Bicarbonate activation of adenylyl cyclase via promotion of catalytic active site closure and metal recruitment. *Nat Struct Mol Biol* 12:32–37.
25. Hammer A, Hodgson DR, Cann MJ (2006) Regulation of prokaryotic adenylyl cyclases by CO_2. *Biochem J* 396:215–218.
26. Hennon GMM, et al. (2015) Diatom acclimation to elevated CO_2 via cAMP signalling and coordinated gene expression. *Nat Clim Chang* 5:761–765.
27. Hood RD, Higgins SA, Flamholz A, Nichols RJ, Savage DF (2016) The stringent response regulates adaptation to darkness in the cyanobacterium *Synechococcus elongatus*. *Proc Natl Acad Sci USA* 113:E4867–E4876.
28. Puszynska AM, O'Shea EK (2017) ppGpp controls global gene expression in light and in darkness in *S. elongatus*. *Cell Rep* 21:3155–3165.
29. Schwarz D, et al. (2011) Metabolic and transcriptomic phenotyping of inorganic carbon acclimation in the cyanobacterium *Synechococcus elongatus* PCC 7942. *Plant Physiol* 155:1640–1655.
30. Heinrich A, et al. (2006) Interaction of the membrane-bound GlnK-AmtB complex with the master regulator of nitrogen metabolism TnrA in *Bacillus subtilis*. *J Biol Chem* 281:34909–34917.
31. Radchenko MV, Thornton J, Merrick M (2010) Control of AmtB-GlnK complex formation by intracellular levels of ATP, ADP, and 2-oxoglutarate. *J Biol Chem* 285: 31037–31045.
32. Huergo LF, et al. (2006) Interactions between P_{II} proteins and the nitrogenase regulatory enzymes DraT and DraG in *Azospirillum brasilense*. *FEBS Lett* 580:5232–5236.
33. Sassone-Corsi P (2012) The cyclic AMP pathway. *Cold Spring Harb Perspect Biol* 4: a011148.
34. Ohmori M, Okamoto S (2004) Photoresponsive cAMP signal transduction in cyanobacteria. *Photochem Photobiol Sci* 3:503–511.
35. Forcada-Nadal A, Forchhammer K, Rubio V (2014) SPR analysis of promoter binding of *Synechocystis* PCC6803 transcription factors NtcA and CRP suggests cross-talk and sheds light on regulation by effector molecules. *FEBS Lett* 588:2270–2276.
36. Nambi S, Basu N, Visweswariah SS (2010) cAMP-regulated protein lysine acetylases in mycobacteria. *J Biol Chem* 285:24313–24323.
37. Vagin A, Teplyakov A (2010) Molecular replacement with MOLREP. *Acta Crystallogr D Biol Crystallogr* 66:22–25.
38. Orf I, et al. (2015) Integrated analysis of engineered carbon limitation in a quadruple CO_2/HCO_3^- uptake mutant of *Synechocystis* sp. PCC 6803. *Plant Physiol* 169:1787–1806.
39. Pinto FL, Thapper A, Sontheim W, Lindblad P (2009) Analysis of current and alternative phenol based RNA extraction methodologies for cyanobacteria. *BMC Mol Biol* 10:79.
40. Imashimizu M, Yoshimura H, Katoh H, Ehira S, Ohmori M (2005) NaCl enhances cellular cAMP and upregulates genes related to heterocyst development in the cyanobacterium, *Anabaena* sp. strain PCC 7120. *FEMS Microbiol Lett* 252:97–103.